CARBON letters

Original Articles
Carbon Letters Vol. 25, 84-88 (2018)

Modulator of surface plasmon polariton based cycle branch graphene waveguide

Jun Zhu[1,2,♠], Zhengjie Xu[1], Wenju Xu[1] and Duqu Wei[1]

[1]College of Electronic Engineering, Guangxi Normal University, Guilin 541004, China
[2]Guangxi Key Laboratory of Automatic Detecting Technology and Instruments, Guilin University of Electronic Technology, Guilin, 541004, China

Article Info

Received 25 May 2017
Accepted 4 September 2017

♠Corresponding Author
E-mail: zhujun1985@gxnu.edu.cn

Open Access

DOI: http://dx.doi.org/10.5714/CL.2018.25.084

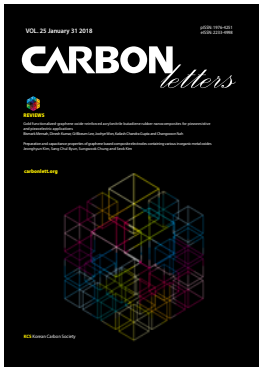

http://carbonlett.org

pISSN: 1976-4251
eISSN: 2233-4998

Abstract

At present, an important research area is the search for materials that are compatible with CMOS technology and achieve a satisfactory response rate and modulation efficiency. A strong local field of graphene surface plasmon polariton (SPP) can increase the interaction between light and graphene, reduce device size, and facilitate the integration of materials with CMOS. In this study, we design a new modulator of SPP-based cycle branch graphene waveguide. The structure comprises a primary waveguide of graphene–$LiNbO_3$–graphene, and a secondary cycle branch waveguide is etched on the surface of $LiNbO_3$. Part of the incident light in the primary waveguide enters the secondary waveguide, thus leading to a phase difference with the primary waveguide as reflected at the end of the branch and interaction coupling to enhance output light intensity. Through feature analysis, we discover that the area of the secondary waveguide shows significant localized fields and SPPs. Moreover, the cycle branch graphene waveguide can realize gain compensation, reduce transmission loss, and increase transmission distance. Numerical simulations show that the minimum effective mode field area is about $0.0130\lambda^2$, the gain coefficient is about 700 cm^{-1}, and the quality factor can reach 150. The structure can realize the mode field limits of deep subwavelength and achieve a good comprehensive performance.

Key words: graphene surface plasmon polariton, modulator, subwavelength, mode field limits

1. Introduction

An electro-optic modulator (EOM) consists of a crystal, such as lithium niobate, gallium arsenide, and lithium tantalite [1,2]. The electro-optic effect is the change in the refractive index of a crystal resulting from the change of light properties. Modulation may be imposed on the phase, frequency, amplitude, or polarization of beams [3,4]. Optical modulators serve as the most important element in optical signal processing systems [5-8]. The development of an integrated optical modulator is aimed at achieving high-speed exploration, wide bandwidth, and small size. Thus, relevant research should be conducted to discover materials that can promote the response rate and modulation efficiency of optical modulators. Graphene is known to have optical properties that favor optical modulation [9-11]. Photons can be readily coupled to surface plasmons in graphene and form a surface plasmon polariton (SPP) surface wave with numerous appealing properties, such as interaction between light and graphene and increased bandwidth [12-14]. Gao's team in the William Marsh Rice University Department of Electrical and Computer Engineering recently revealed that graphene can be used in electric communication, including in Mid and Fir regions. In "Double-Layer Graphene Optical Modulator" published in *Nano Letter*, Zhang Xiang , NAE number, explained the great influence of developing a graphene optical modulator. At present, few studies have reported

on narrow-band filters, and most of them focus on the structural design of graphene modulators. On the basis of the presented overview, we design a new modulator of SPP-based cycle branch graphene waveguide. The structure comprises a primary waveguide of graphene–$LiNbO_3$–graphene, and a secondary cycle branch waveguide is etched on the surface of $LiNbO_3$ [15-18]. We find that the area of the secondary waveguide shows significant localized fields and SPPs. The cycle branch graphene waveguide can realize gain compensation, reduce transmission loss, and increase transmission distance. The structure can realize the mode field limits of deep subwavelengths and achieve a good comprehensive performance.

2. Experimental

2.1. Structure design

We propose a modulator with high extinction ratio and small size (Fig. 1). This modulator can be modulated easily by changing the light of phase, frequency, amplitude, or polarization. It can also be rapidly identified by EOM. At the same time, the modulator features a simple, low-cost system that is easy to develop. Graphene SPP modulators exhibit a periodic structure consisting of upper and lower symmetries. The electrodes are made of galvanized sheet. The main waveguide is based on a material with a graphene–lithium niobate–graphene structure covered with a periodic structure on the surface of the lithium niobate sheet. The branch waveguide, which is used as the gain medium, can boost the localization effect in SPPs. The incident light transfers from the main waveguide to the branch waveguide, thereby leading to a phase difference. Under such condition, the light couples and changes. As a result of the electro-optic effect, the light signal can be modulated and integrated by changing the parameter in the branch waveguide structure. According to this setup, the work frequency can be controlled precisely.

The main waveguide and branch waveguide consist of lithium niobate crystal and covered with graphene at the bottom and on both sides. The branch waveguide, which is adopted for the IR-140-DMSO mixed solution, serves as the gain medium. After modulation, the output light interacts through the graphene and branch structure. The modulator design, which exhibits constructive interference and a periodic change in the cancellation process, allows the control of extinction ratio through the applied voltage and change in branch length. The waveguide design shows a typical symmetric SPP structure. Both sides can produce SPP resonance, thus promoting the ability to absorb light. Graphene can be manufactured with a banded structure via chemical vapor deposition.

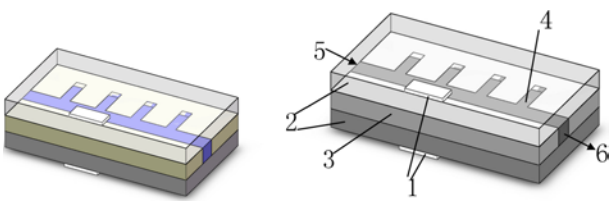

Fig. 1. Modulator with high extinction ratio and small size (1. galvanized sheet, 2. graphene, 3. lithium niobate, 4. branch waveguide, 5. incident light, 6. output light).

Under hierarchical mutual coverage, the periodic structure is covered with graphene, and electrodes are deposited on the graphene surface with the evaporating electron beam. A branched waveguide is obtained via plasma beam sputter etching. The modulator constructed with graphene exhibits outstanding properties, including low loss and good conduction. It can overcome the noise loss that occurs in spontaneous emission in the communication channel. In incident wavelength determination, the output light can be easily controlled by changing the gate voltage on both sides of graphene. At the same time, the filtering characteristics in the branch waveguide can be determined according to specific parameters. In this way, light frequency can be easily controlled. The proposed graphene-based EOM shows excellent extinction rate and modulation efficiency, thereby providing an ideal subwavelength micronano device in large-scale integrated optical communication.

2.2. Propagation analysis

To define the mode field limits of the SPP waveguide on the basis of the size of the subwavelength, we denote the normalized mode scaling factor as SF, which is the ratio between the effective mode field area A_{eff} and the diffraction limit model A_0. Propagation loss is denoted as Loss. SF describes the concentration of the spatial distribution of the electric field energy. A small SF indicates a strong light field constraint ability.

$$SF = A_{eff} / A_0 \tag{1}$$

$$A_{eff} = \frac{1}{\max\left(W(x,y)\right)} \iint W(x,y)\,dxdy \tag{2}$$

$$W(x,y) = \frac{1}{2}\left[\mathrm{Re}\left(\frac{d\left(\varepsilon(x,y)\omega\right)}{d\omega} \right) \left|E(x,y)\right|^2 + u_0 \left|H(x,y)\right|^2 \right] \tag{3}$$

$$A_0 = \lambda^2 / 4\,, \tag{4}$$

W(x,y) is the electromagnetic energy density, $\varepsilon(x,y)$ is the relative dielectric constant, and u_0 is the vacuum magnetic permeability. $E(x,y)$ and $H(x,y)$ denote the electric field and magnetic field, respectively. ω is the angular frequency, and λ is the wavelength. Under the condition of invariable local form, transmission loss is as small as possible. *Loss* is expressed as

$$Loss = -20\lg(e)\, n_{im} k_0 \approx -2 \times n_{im} k_0 \times 4.34\,, \tag{5}$$

Here, n_{im} is the imaginary part of the complex refractive index of the model, and k_0 is the wave number in vacuum, $k_0 = 2\pi/\lambda$. The coefficient of 4.34 ranges from 1 μm^{-1} to dB μm^{-1}. Eq. 5 indicates that the transmission loss is negative when the gain is positive.

In the design of the waveguide, we aim to generate a small transmission loss and a normalized mode field area. Thus, we must analyze the quality factor (*FOM*) to determine the comprehensive transmission characteristics of the waveguide, $FOM = \frac{L}{SF}$. A great *FOM* indicates that the waveguide is applicable in optical transmission. L is the transmission length, which describes

the propagation distance of light in the waveguide structure. L is expressed as

$$L = \frac{1}{2\,\mathrm{Im}(\beta)} \tag{6}$$

Here, β is the mode propagation constant, $\beta = k_0 \frac{\varepsilon_{1i}}{2\varepsilon_{1r}^{\,2}} \left(\frac{\varepsilon_{1r}\varepsilon_2}{\varepsilon_{1r}+\varepsilon_2}\right)^{\frac{3}{2}}$.

ε_{1r} and ε_{1i} are the real part and imaginary part of the metal dielectric constant, respectively. ε_2 is the dielectric constant of the medium in contrast to the symbol of ε_{1r}.

3. Results and Discussion

3.1. Analysis of SPP

We first put forward the SPP characteristics of the modulator. We use a non-electrode in our SPP analysis. The analysis conditions are as follows: the incident wavelength is 1550 nm, the structure is 200 nm in length, the primary waveguide is 40 nm thick, and the secondary cycle branch waveguide is 30 nm thick. The width of the modulator is 150 nm thick. Fig. 2 shows the results with electric field distribution, transverse electric field, and longitudinal electric field. As shown in the figure, the area of the branch has significant localized fields, in which the coupling between the branch model and primary waveguide mode occurs and SPP is realized. In the area of the apex angle branch, resonance intensity is obviously the greatest. The clearance between the graphene and the medium waveguide with a high refractive index can be confined to the mode field, where light field limits are achieved.

The result also shows that the graphene-based cycle branch waveguide can realize gain compensation, reduce transmission loss, and increase transmission distance. The energy is limited to a small area in the horizontal and vertical directions. In comparison with the traditional metal–insulator–metal structure, the designed structure shows a stronger horizontal field limiting ability.

3.2. Analysis of cycle branch

To further clarify the effect of the waveguide structure on the spread of the SPPs, we use the condition of 3.1, in addition to changing the structure of the branch size. Fig. 3 shows the result of the analysis of the resulting localized electric field: (a) 20, (b) 30, (c) 40, (d) 50, (e), 60, (f) 70, (g) 80, (h) 90 nm. As shown in the diagram, all branches show strong coupling, and local form is realized.

Fig. 4 shows the result of the analysis of the situation of effective refractive index: 10 nm, 5.7773-0.42373i; 20 nm, 5.4849-0.42314i; 30 nm, 5.1999-0.42618; 40 nm, 4.9197-0.43312i; 50 nm, 4.6427-0.4439i; 60 nm, 4.3688-0.46069i; 70 nm, 4.0948-0.48384i; 80 nm, 3.8215-0.51218i; 90 nm, 3.546-

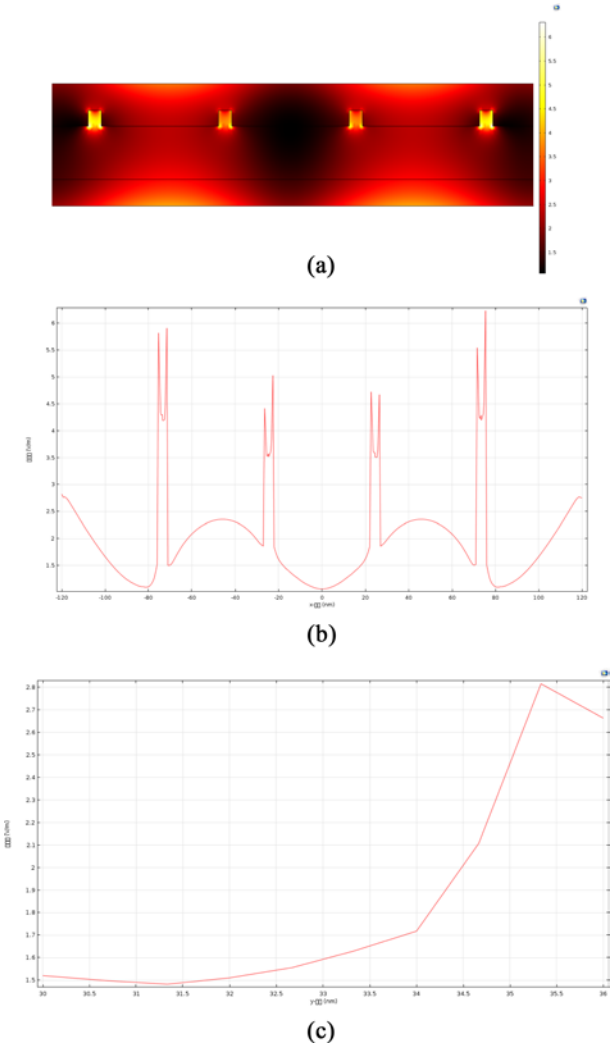

Fig. 2. (a) Electric field localization; (b) transverse electric field; (c) longitudinal electric field.

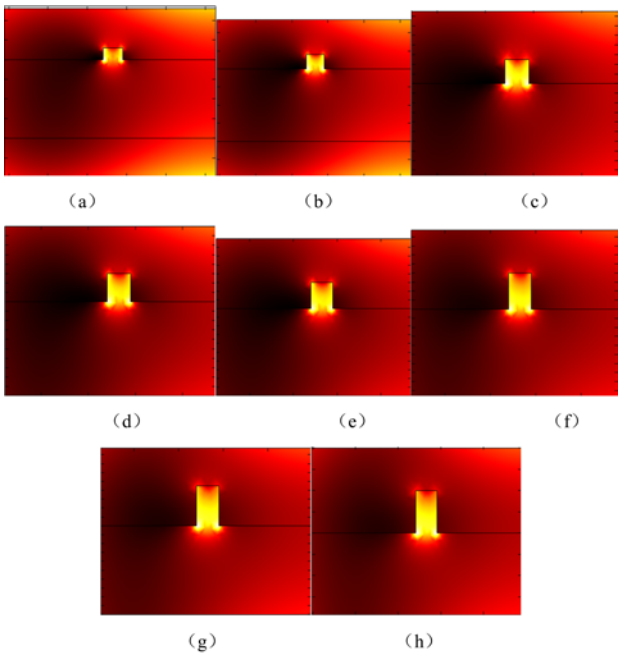

Fig. 3. The situation of electric field localized: (a) 20 nm, (b) 30 nm, (c) 40 nm, (d) 50 nm, (e) 60 nm, (f) 70 nm, (g) 80 nm, (h) 90 nm.

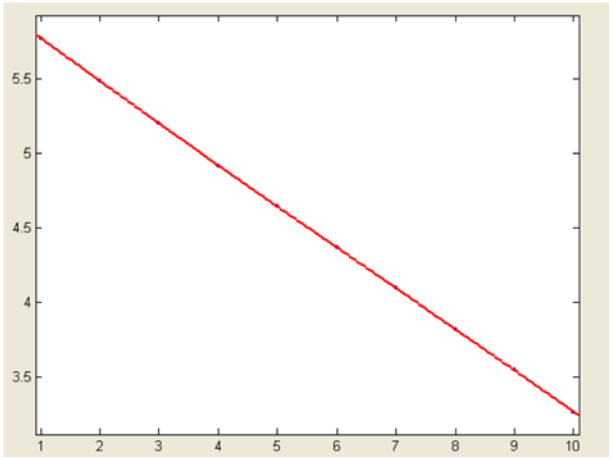

Fig. 4. The situation of effective refractive.

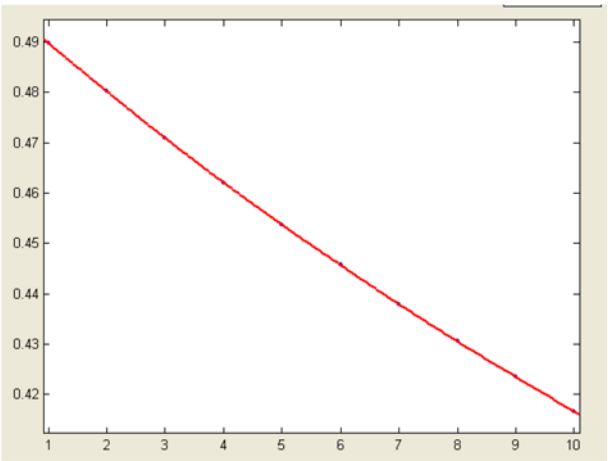

Fig. 6. The situation of limiting factors.

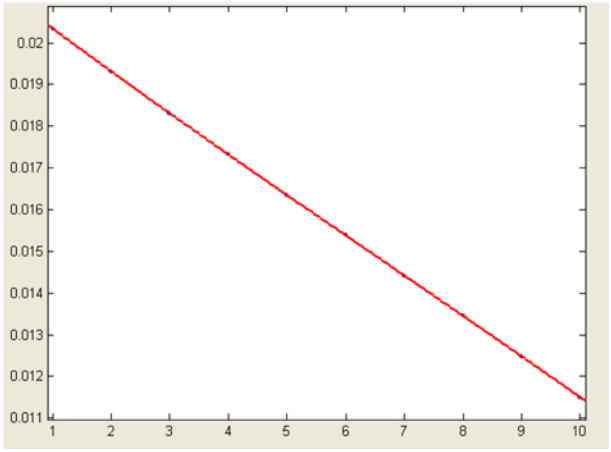

Fig. 5. The situation of propagation loss.

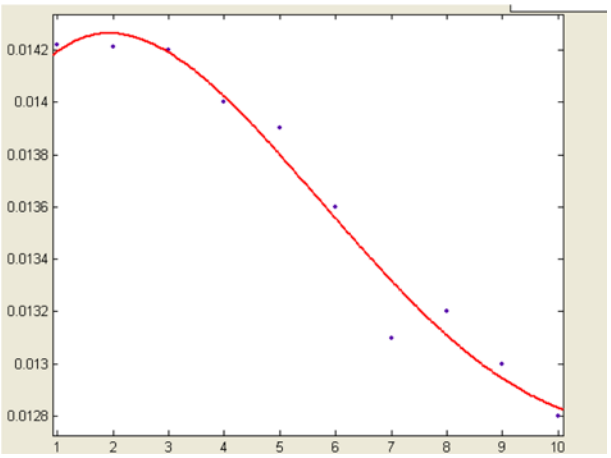

Fig. 7. The situation of normalized effective mode field.

0.55044i. As shown in the diagram, when height of branch increases, effective refractive index decreases.

Fig. 5 shows the result of the analysis of the situation of propagation loss: 10 nm, 0.020342; 20 nm, 0.019312; 30 nm, 0.018308; 40 nm, 0.017322; 50 nm, 0.016347; 60 nm, 0.015382; 70 nm, 0.014418; 80 nm, 0.013455; 90 nm, 0.012485.

Fig. 6 shows the result of the analysis of situation of limiting factors: 10, nm 0.4898; 20 nm, 00.4802; 30 nm, 0.4709; 40 nm, 0.4621; 50 nm, 0.4537; 60 nm, 0.4457; 70 nm, 0.4379; 80 nm, 0.4305; 90 nm, 0.4235.

Fig. 7 shows the result of the analysis of situation of normalized effective mode field: 10 nm, 0.01423; 20 nm, 0.01422; 30 nm, 0.01421; 40 nm, 0.0142; 50 nm, 0.0140; 60 nm 0.0139; 70 nm, 0.0136; 80 nm, 0.0132; 90 nm, 0.0130.

Fig. 8 shows the result of the analysis of the situation of gain threshold: 10 nm, 0.0557; 20 nm, 0.0573; 30 nm, 0.0590; 40 nm, 0.0602; 50 nm, 0.0620; 60 nm, 0.0633; 70 nm, 0.0648; 80 nm, 0.0665; 90 nm, 0.0677.

A comprehensive analysis of Figs. 5-8 reveals that when the height of the branch increases, transmission loss, limiting

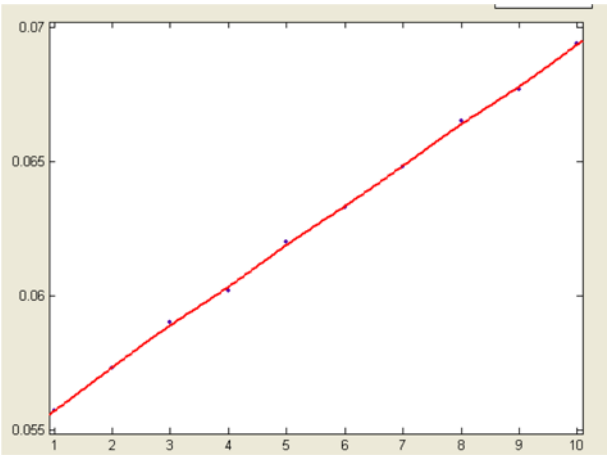

Fig. 8. The situation of gain threshold.

factors, and the normalized effective mode field area decrease, and the gain threshold increases obviously. The minimum

effective mode field area is about $0.0130\lambda^2$, the gain coefficient is about 700 cm^{-1}, and FOM can reach 150. The structure can realize the mode field limits of the deep subwavelength and achieve a good comprehensive performance.

4. Conclusions

In the new modulator of SPP-based cycle branch graphene waveguide, part of the incident light in the primary waveguide enters the secondary waveguide, thus leading to a phase difference with the primary waveguide as reflected at end of the branch and interaction coupling to enhance output light intensity. Numerical simulations show that the minimum effective mode field area is about $0.0130\lambda^2$, the gain coefficient is about 700 cm^{-1}, and the FOM can reach 150. The structure can realize the mode field limits of the deep subwavelength and achieve a good comprehensive performance. The features of the new type of modulator make it compatible with CMOS technology and can thus serve as an integrated unit with obvious application value.

Conflict of Interest

No potential conflict of interest relevant to this article was reported.

Acknowledgements

This work was supported by Guangxi Natural Science Foundation (2017GXNSFAA198261), Guangxi Scholarship Fund of Guangxi Education Department, Guangxi Normal University Key Program(2015ZD03), and Innovation Project of Guangxi Graduate Education(XJGY201811, XJGY201807).

References

[1] Ma HF, Shen X, Cheng Q, Jiang WX, Cui TJ. Broadband and high-efficiency conversion from guided waves to spoof surface plasmon polaritons. Laser Photonics Rev, **8**, 146 (2013). https://doi.org/10.1002/lpor.201300118.

[2] Douillard L, Charra F, Korczak Z, Bachelot R, Kostcheev S, Lerondel G, Adam PM, Royer P. Short range plasmon resonators probed by photoemission electron microscopy. Nano Lett, **8**, 935 (2008). https://doi.org/10.1021/nl080053v.

[3] Zheng G, Mühlenbernd H, Kenney M, Li G, Zentgraf T, Zhang S. Metasurface holograms reaching 80% efficiency. Nat Nanotechnol, **10**, 308 (2015). https://doi.org/10.1038/nnano.2015.2.

[4] Lubart T, Besançon M. On the Measurement and Mismeasurement of Creativity. In: Beghetto R, Sriraman B, eds. Creative Contradictions in Education. Springer, Cham, 333 (2017). https://doi.org/10.1007/978-3-319-21924-0_18.

[5] Gao H, Zheng Z, Dong J, Feng J, Zhou J. Multi-frequency optical unidirectional transmission based on one-way guided mode resonance in an extremely simple dielectric grating. Opt Commun, **355**, 137 (2015). https://doi.org/10.1016/j.optcom.2015.06.038.

[6] Törmä P, Barnes WL. Strong coupling between surface plasmon polaritons and emitters: a review. Rep Prog Phys, **78**, 013901 (2014). https://doi.org/10.1088/0034-4885/78/1/013901.

[7] Bliokh KY, Smirnova D, Nori F. Quantum spin Hall effect of light. Science, **348**, 1448 (2015). https://doi.org/10.1126/science.aaa9519.

[8] Fang Y, Sun M. Nanoplasmonic waveguides: towards applications in integrated nanophotonic circuits. Light Sci Appl, **4**, e294 (2015). https://doi.org/10.1038/lsa.2015.67.

[9] Bartoli FJ, Gao Y, Zeng B. Ultrathin nanostructured metals for highly transmissive plasmonic subtractive color filters. US Patent Application US20150124306A1 (2015).

[10] Piazza L, Lummen TTA, Quiñonez E, Murooka Y, Reed BW, Barwick B, Carbone F. Simultaneous observation of the quantization and the interference pattern of a plasmonic near-field. Nat Commun, **6**, 6407 (2015). https://doi.org/10.1038/ncomms7407.

[11] High AA, Devlin RC, Dibos A, Polking M, Wild DS, Perczel J, de Leon NP, Lukin MD, Park H. Visible-frequency hyperbolic metasurface. Nature, **522**, 192 (2015). https://doi.org/10.1038/nature14477.

[12] Caucheteur C, Guo T, Albert J. Review of plasmonic fiber optic biochemical sensors: improving the limit of detection. Anal Bioanal Chem, **407**, 3883 (2015). https://doi.org/10.1007/s00216-014-8411-6.

[13] Dai S, Ma Q, Liu MK, Andersen T, Fei Z, Goldflam MD, Wagner M, Watanabe K, Taniguchi T, Thiemens M, Keilmann F, Janssen GCAM, Zhu SE, Jarillo-Herrero P, Fogler MM, Basov DN. Graphene on hexagonal boron nitride as a tunable hyperbolic metamaterial. Nat Nanotechnol, **10**, 682 (2015). https://doi.org/10.1038/nnano.2015.131.

[14] Caldwell JD, Lindsay L, Giannini V, Vurgaftman I, Reinecke TL, Maier SA, Glembocki OJ. Low-loss, infrared and terahertz nanophotonics using surface phonon polaritons. Nanophotonics, **4**, 44 (2015). https://doi.org/10.1515/nanoph-2014-0003.

[15] Zhang HC, Liu S, Shen X, Chen LH, Li L, Cui TJ. Broadband amplification of spoof surface plasmon polaritons at microwave frequencies. Laser Photonics Rev, **9**, 83 (2015). https://doi.org/10.1002/lpor.201400131.

[16] Lu H, Zeng C, Zhang Q, Liu X, Hossain MM, Reineck P, Gu M. Graphene-based active slow surface plasmon polaritons. Sci Rep, **5**, 8443 (2015). https://doi.org/10.1038/srep08443.

[17] Yin JY, Ren J, Zhang HC, Pan BC, Cui TJ. Broadband frequency-selective spoof surface plasmon polaritons on ultrathin metallic structure. Sci Rep, **5**, 8165. https://doi.org/10.1038/srep08165.

[18] Senin P. jmotif: Time Series Analysis Toolkit Based on Symbolic Aggregate Dicretization, i.e. SAX. Available from: https://rdrr.io/cran/jmotif/.